Engineering Analysis with Boundary Elements ∎ (∎∎∎∎) ∎∎∎–∎∎∎

Contents lists available at ScienceDirect

Engineering Analysis with Boundary Elements

journal homepage: www.elsevier.com/locate/enganabound

Equivalence between the Trefftz method and the method of fundamental solution for the annular Green's function using the addition theorem and image concept

Jeng-Tzong Chen [a,b,*], Ying-Te Lee [a], Shang-Ru Yu [a], Shiang-Chih Shieh [a]

[a] Department of Harbor and River Engineering, National Taiwan Ocean University, Keelung 20224, Taiwan
[b] Department of Mechanical and Mechatronic Engineering, National Taiwan Ocean University, Keelung 20224, Taiwan

ARTICLE INFO

Article history:
Received 19 May 2008
Accepted 7 October 2008

Keywords:
Green's function
Method of fundamental solutions
Image method
Trefftz method

ABSTRACT

In this paper, the Green's function for the annular Laplace problem is first derived by using the image method which can be seen as a special case of method of fundamental solutions. Three cases, fixed–fixed, fixed–free and free–fixed boundary conditions are considered. Also, the Trefftz method is employed to derive the analytical solution by using T-complete sets. By employing the addition theorem, both solutions are found to be mathematically equivalent when the number of Trefftz base and the number of image points are both infinite. On the basis of the same number of degrees of freedom, the convergence rate of both methods is compared with each other. In the successive image process, the final two images freeze at the origin and infinity, where their singularity strengths can be analytically and numerically determined in a consistent manner.

© 2008 Elsevier Ltd. All rights reserved.

1. Introduction

Trefftz in 1926 presented the Trefftz method for solving boundary value problems (BVPs) by superimposing the functions satisfying the governing equation, although various versions of the Trefftz method, e.g., direct and indirect formulations have been developed [1]. The unknown coefficients are determined by matching the boundary condition. Many applications to the Laplace equation [2], the Helmholtz equation [3], the Navier equation [4,5], and the biharmonic equation [6] were done. Until the recent years, the ill-posed nature in the method was noticed [7].

In the potential theory, it is well known that the method of fundamental solutions (MFS) can solve potential problems when a fundamental solution is known. This method was proposed by Kupradze [8] in Russia. Extensive applications in solving a broad range of problems such as potential problems [9], acoustics [10], elasticity [8] and biharmonic problems (plate) [11–13] have been investigated. The MFS can be viewed as an indirect boundary element method (BEM) with concentrated sources instead of boundary distributions. The initial idea is to approximate the solution through a linear combination of fundamental solutions with sources located outside the domain of the problem. Moreover, it has certain advantages over BEM, e.g., no singularity and no boundary integrals are required. However, ill-posed behavior is inherent in the regular formulation. The Trefftz method and MFS are both mesh reduction methods.

The Green's function has been studied and applied in many fields by mathematicians as well as engineers [14,15]. The Green's functions are useful building blocks for attacking more realistic problems. But only a few of simple regions allow a closed-form Green's function for the Laplace equation. For example, one aperture or circular sector in the half-plane, infinite strip, semi-strip or infinite wedge can be mapped by elementary analytic functions, making their Green's function expressed in a closed form. A closed-form Green's function for the Laplace equation by using the mapping function becomes impossible for the complicated domain except for some simple cases. Numerical Green's function has received attention from BEM researchers by Telles et al. [16–18]. Melnikov [19–21] utilized the method of modified potentials (MMP) to solve BVPs from various areas of computational mechanics. Later, Melnikov and Melnikov [22] studied in computing Green's functions and matrices of Green's type for mixed BVPs stated on 2-D regions of irregular configuration. For the image method, Thompson [23] proposed the concept of reciprocal radii to find the image source to satisfy the homogeneous Dirichlet boundary condition. Chen and Wu [24] proposed an alternative way to find the location of image by employing the degenerate kernel. Boley [25] analytically con-

* Corresponding author at: Department of Harbor and River Engineering, National Taiwan Ocean University, Keelung 20224, Taiwan. Tel.:+886 2 24622192 x6177; fax: +886 2 24632375.
E-mail address: jtchen@mail.ntou.edu.tw (J.-T. Chen).

0955-7997/$ - see front matter © 2008 Elsevier Ltd. All rights reserved.
doi:10.1016/j.enganabound.2008.10.003

structed the Green's function by using the successive approximation. Adewale [26] proposed an analytical solution for an annular plate subjected to a concentrated load which also belongs to the Green's function. Chen and Ke [27] have constructed the Green's function of Helmholtz operator domain by using the null-field integral equation derived from the Green's third identity. The Green's function of a circular ring has been solved using complex variable by Courant and Hilbert [28]. However, it is limited to extend to 3-D space.

Mathematical studies on MFS have been investigated by some researchers. Schabck [29] found that the MFS with far field singularity behaves like the Trefftz base of harmonic polynomials. Bogomolny [30] studied the stability and error bound of MFS. Li et al. [31] used the effective condition number to study the collocation approaches of MFS and Trefftz method. He found that the condition number of MFS is much worst than that of the Trefftz method. Although the Trefftz method and MFS have a long history individually, the link between the two methods was not discussed in detail in the literature until Chen et al.'s paper [32]. They proved the equivalence between the Trefftz method and the MFS for Laplace and biharmonic problems containing the circular domain. The key point is the use of the degenerate kernel or so-called the addition theorem. They only proved the equivalence by demonstrating a simple circle with angular distribution of singularity to link the two methods. However, an extension study for a doubly connected problem is not trivial. This is the main concern of this paper. Here, we put singularities along the radial direction in the method of image.

In this paper, we focus on proving the mathematical equivalence on the Green's functions for annular Laplace problem derived by using the Trefftz method and MFS. Three cases fixed–fixed, fixed–free and free–fixed boundary conditions are considered. By employing the image method and addition theorem, the equivalence of the two methods will be proved when the number of image points and number of the Trefftz bases are infinite. The image method is seen as a special case of MFS, since its image singularities locate outside the domain. The convergence rate on the basis of same number of degrees of freedoms for the Trefftz method and MFS is also discussed. The solution by using the image method also indicates that a free constant is required to be complete for the solution which is always neglected in the conventional MFS.

2. Construction of the Green's function for an annular case by using the image method

For a 2-D annular problem as shown in Fig. 1, the Green's function satisfies

$$\nabla^2 G(x,\zeta) = \delta(x-\zeta), \quad x \in \Omega, \tag{1}$$

where Ω is the domain of interest and δ denotes the Dirac-delta

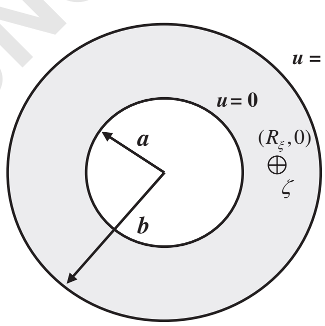

Fig. 1. Sketch of an annular problem subject to a concentrated load.

function for the source at ζ. For simplicity, the Green's function is considered to be subjected to the Dirichlet boundary condition

$$G(x,\zeta) = 0, \quad x \in B_1 \cup B_2, \tag{2}$$

where B_1 and B_2 are the inner and outer boundaries, respectively. As mentioned in [24], the interior and exterior Green's functions can satisfy the homogeneous Dirichlet boundary conditions if the image source is correctly selected. The closed-form Green's functions for both interior and exterior problems are written to be the same form

$$G(x,\zeta) = \ln|x-\zeta| - \ln|x-\zeta'| + \ln a - \ln R_\zeta, \quad x \in \Omega, \tag{3}$$

where a is the radius of the circle, $\zeta = (R_\zeta, 0)$, R_ζ is the distance from the source to the center of the circle, ζ is the image source and its position is at $(a^2/R_\zeta, 0)$ as shown in Fig. 2.

Now let us extend a circular case to an annular case. An annular case can be seen as a combination of interior problem and exterior problem as shown in Fig. 3. By matching the homogeneous Dirichlet boundary conditions for the inner and outer boundaries (fixed–fixed case), we introduce image points ζ_1 and ζ_2, respectively. Since ζ_2 results in the nonhomogeneous boundary conditions on the outer boundary, we need to introduce an extra image point ζ_3. Similarly, ζ_1 results in the nonhomogeneous boundary conditions on the inner boundary and an additional image point ζ_4 are also required. By repeating the same procedures, we have a series of image sources locating at

$$\zeta_1 = \frac{b^2}{R_\xi}, \quad \zeta_3 = \frac{a^2}{b^2}R_\xi, \quad \zeta_5 = \frac{b^4}{a^2 R_\xi}, \quad \zeta_7 = \frac{a^4}{b^4}R_\xi, \ldots,$$
$$\zeta_{4i-3} = \left(\frac{b^2}{a^2}\right)^{i-1}\left(\frac{b^2}{R_\xi}\right), \quad \zeta_{4i-1} = \left(\frac{a^2}{b^2}\right)^{i} R_\xi, \quad i \in N, \tag{4}$$

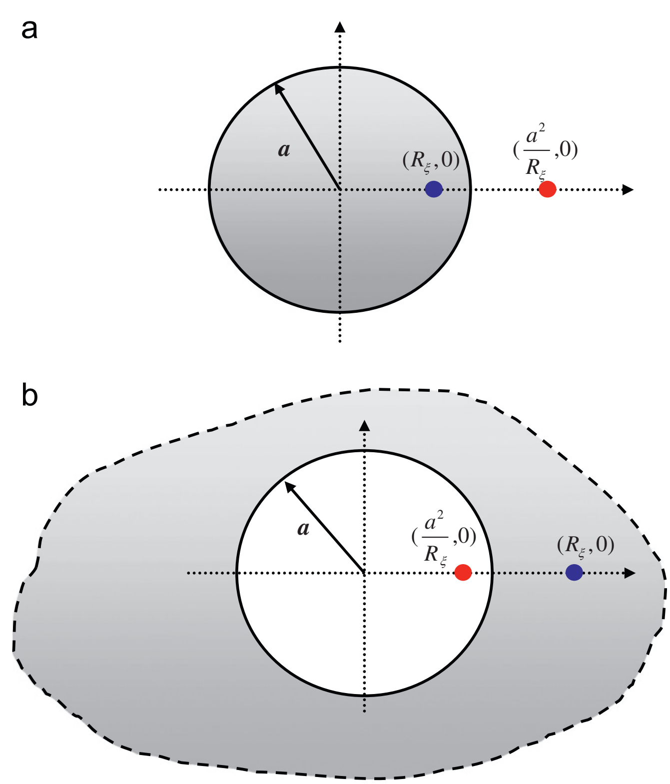

Fig. 2. Sketch of position of image point (a) interior case and (b) exterior case.

UNCORRECTED PROOF

Please cite this article as: Chen J-T, et al. Equivalence between the Trefftz method and the method of fundamental solution for the annular Green's.... Eng Anal Bound Elem (2008), doi:10.1016/j.enganabound.2008.10.003

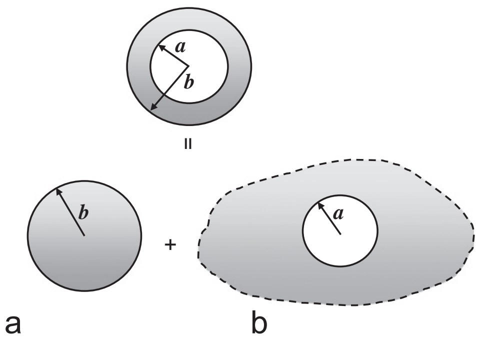

Fig. 3. An annular problem composed of (a) interior and (b) exterior cases.

$$\zeta_2 = \frac{a^2}{R_\xi},\quad \zeta_4 = \frac{b^2}{a^2}R_\xi,\quad \zeta_6 = \frac{a^4}{b^2 R_\xi},\quad \zeta_8 = \frac{b^4}{a^4}R_\xi,\ldots,$$

$$\zeta_{4i-2} = \left(\frac{a^2}{b^2}\right)^{i-1}\left(\frac{a^2}{R_\xi}\right),\quad \zeta_{4i} = \left(\frac{b^2}{a^2}\right)^{i} R_\xi,\quad i\in N. \tag{5}$$

Fig. 4 and Table 1 depicts a series of images for the three annular problems. We consider the fundamental solution $U(s,x)$ for each source singularity which satisfies

$$\nabla^2 U(x,s) = 2\pi\delta(x-s). \tag{6}$$

Then, we obtain the fundamental solution as follows:

$$U(x,s) = \ln r, \tag{7}$$

where r is the distance between s and x ($r\equiv|x-s|$). Based on the separable property of addition theorem or degenerate kernel, the fundamental solution $U(x,s)$ can be expanded into series form by separating the field point $x(\rho,\phi)$ and source point $s(R,\theta)$ in the polar coordinate [33]

$$U(s,x) = \begin{cases} U^I(R,\theta;\rho,\phi) = \ln R - \sum_{m=1}^{\infty}\frac{1}{m}\left(\frac{\rho}{R}\right)^m \cos m(\theta-\phi), & R\geqslant\rho, \\ U^E(R,\theta;\rho,\phi) = \ln\rho - \sum_{m=1}^{\infty}\frac{1}{m}\left(\frac{R}{\rho}\right)^m \cos m(\theta-\phi), & R<\rho, \end{cases} \tag{8}$$

where the superscripts of I and E denote the interior and exterior regions, respectively. It is noted that the leading term and the numerator in the above expansion involve the larger argument to ensure the log singularity and the series convergence, respectively. In order to iteratively match the inner and outer homogenous Dirichlet boundary conditions, combination of all the images yields a part of the Green's function

$$G_m(x,\zeta) = \frac{1}{2\pi}\left[\ln|x-\zeta| - \lim_{N\to\infty}\sum_{i=1}^{N}(\ln|x-\zeta_{4i-3}| + \ln|x-\zeta_{4i-2}| - \ln|x-\zeta_{4i-1}| - \ln|x-\zeta_{4i}|)\right]. \tag{9}$$

2.1. Satisfaction of boundary conditions using two singularity strengths at the origin and infinity

After successive image process, the final two image locations freeze at the origin and infinity. There are two strength of singularity to be determined. Therefore, the total Green's function is rewritten as

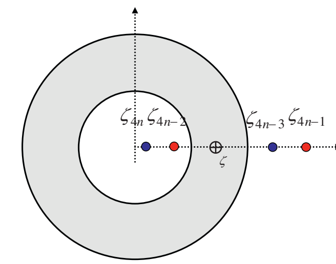

Fig. 4. The images for an annular problem.

$$G(x,\zeta) = \lim_{N\to\infty}\left\{\frac{1}{2\pi}\left[\ln|x-\zeta| - \sum_{i=1}^{N}(\ln|x-\zeta_{4i-3}| + \ln|x-\zeta_{4i-2}| - \ln|x-\zeta_{4i-1}| - \ln|x-\zeta_{4i}|) ** \frac{1}{2\pi} **\right] + c(N) + d(N)\ln\rho\right\}, \tag{10}$$

where $c(N)$ and $d(N)$ are unknown coefficients which can be analytically and numerically determined by matching the inner and outer boundary conditions.

After matching the inner and outer boundary conditions, the numerical values of unknown $c(N)$ and $d(N)$ are determined as shown in Figs. 5–7 for fixed–fixed, fixed–free and free–fixed cases, respectively. It is found that all the numerical values in Figs. 5–7 match well with the analytical formulae of $c(N)$ and $d(N)$ in the Table 1 derived by using the degenerate kernel.

2.2. Satisfaction of the boundary condition by using interpolation functions

Although $G_m(x,\zeta)$ is the main part of the Green's function. Unfortunately, $G_m(x,\zeta)$ in Eq. (9) cannot satisfy both the inner and outer boundary conditions of $G_m(x_a,\zeta) = G_m(x_b,\zeta) = 0$, where $x_a = (a,\phi)$, $x_b = (b,\phi)$, $0\leqslant\phi\leqslant 2\pi$. In order to satisfy both the inner and outer boundary conditions, an alternative method is introduced such that we have

$$G(x,\zeta) = G_m(x,\zeta) - \left(\frac{\ln\rho - \ln a}{\ln b - \ln a}\right)G_m(x_b,\zeta) - \left(\frac{\ln b - \ln\rho}{\ln b - \ln a}\right)G_m(x_a,\zeta),\quad a\leqslant\rho\leqslant b, \tag{11}$$

where $((\ln\rho - \ln a)/(\ln b - \ln a))$ and $((\ln b - \ln\rho)/(\ln b - \ln a))$ are the interpolation functions. Therefore, Eq. (11) can be rewritten as

$$\begin{aligned} G(x,\zeta) = \lim_{N\to\infty}\Bigg\{ & \frac{1}{2\pi}\left[\ln|x-\zeta| - \sum_{i=1}^{N}(\ln|x-\zeta_{4i-3}| + \ln|x-\zeta_{4i-2}| - \ln|x-\zeta_{4i-1}| - \ln|x-\zeta_{4i}|)\right] \\ & - \frac{1}{2\pi}\left(\frac{\ln\rho - \ln a}{\ln b - \ln a}\right)\left(\ln b\left(\frac{R_\zeta^2}{a^2}\right)^N - \sum_{m=1}^{\infty}\frac{1}{m}\left[\left(\frac{a^2}{b^2}\right)^N \frac{R_\zeta}{b}\right]^m \cos m(\theta-\phi)\right) \\ & - \frac{1}{2\pi}\left(\frac{\ln b - \ln\rho}{\ln b - \ln a}\right)\left(\ln R_\zeta\left(\frac{R_\zeta^2}{a^2}\right)^N - \sum_{m=1}^{\infty}\frac{1}{m}\left[\left(\frac{a^2}{b^2}\right)^N \frac{a}{R_\zeta}\right]^m \cos m(\theta-\phi)\right)\Bigg\}, \end{aligned} \tag{12}$$

after expanding the fundamental solutions of G_m in Eq. (9) by using the addition theorem. As N approaches infinity (i.e. many image points), $\lim_{N\to\infty}(a^2/b^2)^N$ approaches zero such that Eq. (12) can be reduced to

UNCORRECTED PROOF

Please cite this article as: Chen J-T, et al. Equivalence between the Trefftz method and the method of fundamental solution for the annular Green's.... Eng Anal Bound Elem (2008), doi:10.1016/j.enganabound.2008.10.003

Table 1
Trefftz and image solutions for the fixed–fixed, fixed–free and free–fixed annular Green's functions..

Method	a	b	c
	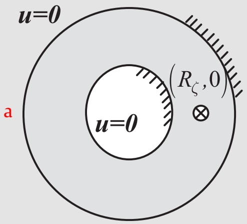	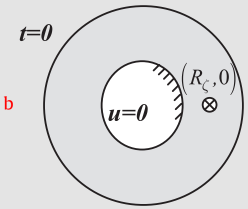	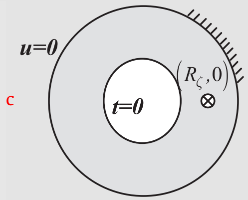
Trefftz solution	$G(x,\zeta)=\frac{\ln\lvert x-\zeta\rvert}{2\pi}+p_0+\bar{p}_0\ln\rho+\sum_{m=1}^{\infty}[p_m\rho^m\cos m\theta+q_m\rho^m\sin m\theta+\bar{p}_m\rho^{-m}\cos m\theta+\bar{q}_m\rho^{-m}\sin m\theta]$		
$\begin{Bmatrix}p_0\\ \bar{p}_0\end{Bmatrix}$	$\begin{bmatrix}\frac{-\ln b(\ln a-\ln R_\zeta)}{2\pi(\ln a-\ln b)}\\ \frac{-(\ln b-\ln R_\zeta)}{2\pi(\ln b-\ln a)}\end{bmatrix}$	$\begin{bmatrix}\frac{\ln a-\ln R_\zeta}{2\pi}\\ \frac{-1}{2\pi}\end{bmatrix}$	$\begin{bmatrix}-\frac{1}{2\pi}\ln b\\ 0\end{bmatrix}$
$\begin{Bmatrix}p_m\\ \bar{p}_m\end{Bmatrix}$	$\begin{bmatrix}\frac{\cos m\theta[R_\zeta^m-a^m(a/R_\zeta)^m]}{2m\pi(b^{2m}-a^{2m})}\\ \frac{a^mb^m\cos m\theta[b^m(a/R_\zeta)^m-a^m(R_\zeta/b)^m]}{2m\pi(b^{2m}-a^{2m})}\end{bmatrix}$	$\begin{bmatrix}\frac{\cos m\theta[a^m(a/R_\zeta)^m-R_\zeta^m]}{2m\pi(b^{2m}+a^{2m})}\\ \frac{a^mb^m\cos m\theta[b^m(a/R_\zeta)^m+a^m(R_\zeta/b)^m]}{2m\pi(b^{2m}+a^{2m})}\end{bmatrix}$	$\begin{bmatrix}\frac{\cos m\theta[R_\zeta^m+a^m(a/R_\zeta)^m]}{2m\pi(b^{2m}+a^{2m})}\\ \frac{-a^mb^m\cos m\theta[b^m(a/R_\zeta)^m-a^m(R_\zeta/b)^m]}{2m\pi(b^{2m}+a^{2m})}\end{bmatrix}$
$\begin{Bmatrix}q_m\\ \bar{q}_m\end{Bmatrix}$	$\begin{bmatrix}\frac{a^mb^m\sin m\theta[b^m(a/R_\zeta)^m-a^m(R_\zeta/b)^m]}{2m\pi(b^{2m}-a^{2m})}\\ \frac{\sin m\theta[b^m(R_\zeta/b)^m-a^m(a/R_\zeta)^m]}{2m\pi(b^{2m}-a^{2m})}\end{bmatrix}$	$\begin{bmatrix}\frac{\sin m\theta[a^m(a/R_\zeta)^m-R_\zeta^m]}{2m\pi(b^{2m}+a^{2m})}\\ \frac{a^mb^m\sin m\theta[b^m(a/R_\zeta)^m+a^m(R_\zeta/b)^m]}{2m\pi(b^{2m}+a^{2m})}\end{bmatrix}$	$\begin{bmatrix}\frac{\sin m\theta[R_\zeta^m+a^m(a/R_\zeta)^m]}{2m\pi(b^{2m}+a^{2m})}\\ \frac{-a^mb^m\sin m\theta[b^m(a/R_\zeta)^m-a^m(R_\zeta/b)^m]}{2m\pi(b^{2m}+a^{2m})}\end{bmatrix}$
Image solution	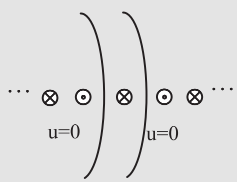	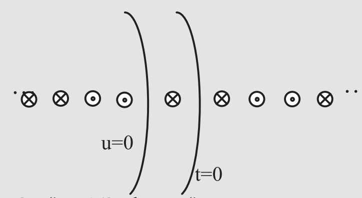	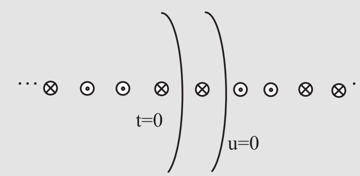
	$G(x,\zeta)=1/2\pi\{\ln\lvert x-\zeta\rvert-\sum_{n=1}^{N}[\ln\lvert x-\zeta_{4n-3}\rvert+\ln\lvert x-\zeta_{4n-2}\rvert-\ln\lvert x-\zeta_{4n-1}\rvert-\ln\lvert x-\zeta_{4n}\rvert]-(2N\ln(R_\zeta/a)+\ln b(\ln a-\ln R_\zeta/\ln a-\ln b))-(\ln b-\ln R_\zeta/(\ln b-\ln a))\ln\rho\},\ a\leqslant\rho\leqslant b$	$G(x,\zeta)=1/2\pi\{\ln\lvert x-\zeta\rvert+\sum_{n=1}^{N}[\ln\lvert x-\zeta_{8n-7}\rvert-\ln\lvert x-\zeta_{8n-6}\rvert-\ln\lvert x-\zeta_{8n-5}\rvert-\ln\lvert x-\zeta_{8n-4}\rvert-\ln\lvert x-\zeta_{8n-3}\rvert+\ln\lvert x-\zeta_{8n-2}\rvert+\ln\lvert x-\zeta_{8n-1}\rvert+\ln\lvert x-\zeta_{8n}\rvert]+\ln a-\ln R_\zeta-\ln\rho\},\quad a\leqslant\rho\leqslant b$	$G(x,\zeta)=1/2\pi\{\ln\lvert x-\zeta\rvert+\sum_{n=1}^{N}[-\ln\lvert x-\zeta_{8n-7}\rvert+\ln\lvert x-\zeta_{8n-6}\rvert-\ln\lvert x-\zeta_{8n-5}\rvert-\ln\lvert x-\zeta_{8n-4}\rvert+\ln\lvert x-\zeta_{8n-3}\rvert-\ln\lvert x-\zeta_{8n-2}\rvert+\ln\lvert x-\zeta_{8n-1}\rvert+\ln\lvert x-\zeta_{8n}\rvert]-(\ln b+4N\ln(b/a))\},\quad a\leqslant\rho\leqslant b$
$c(N)$	$-\left(2N\ln\frac{R_\zeta}{a}+\ln b\frac{\ln a-\ln R_\zeta}{\ln a-\ln b}\right)$	$\ln a-\ln R_\zeta$	$-\left(\ln b+4N\ln\frac{b}{a}\right)$
$d(N)$	$-\frac{\ln b-\ln R_\zeta}{(\ln b-\ln a)}$	-1	0

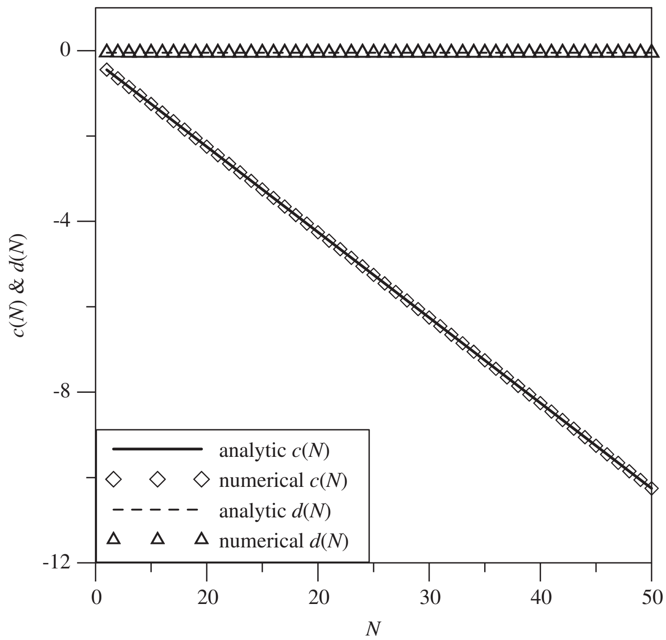

Fig. 5. Values of $c(N)$ and $d(N)$ for the fixed–fixed case.

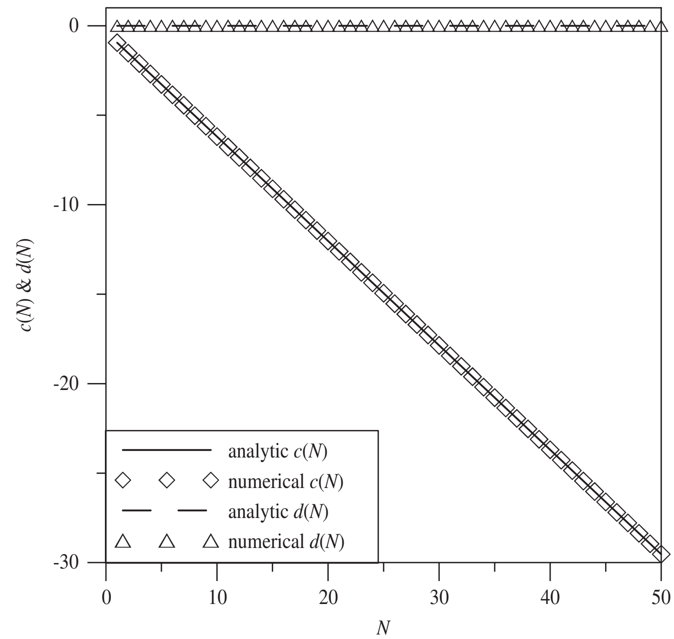

Fig. 7. Values of $c(N)$ and $d(N)$ for the free–fixed case.

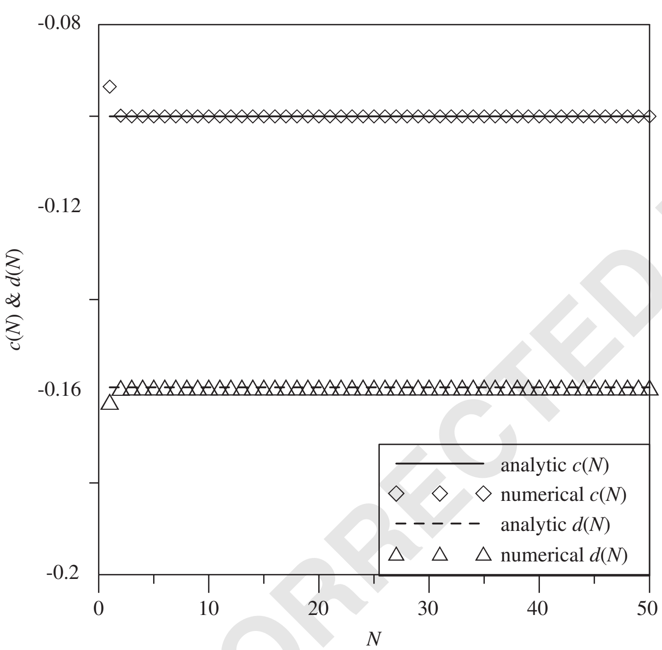

Fig. 6. Values of $c(N)$ and $d(N)$ for the fixed–free case.

$$G(x,\zeta)=\lim_{N\to\infty}\left\{\frac{1}{2\pi}\left[\ln|x-\zeta|-2N\ln\frac{R_\zeta}{a}-\left(\frac{\ln R_\zeta-\ln a}{\ln b-\ln a}\right)\ln b-\left(\frac{\ln b-\ln R_\zeta}{\ln b-\ln a}\right)\ln\rho\right]-\frac{1}{2\pi}\sum_{i=1}^{N}(\ln|x-\zeta_{4i-3}|+\ln|x-\zeta_{4i-2}|-\ln|x-\zeta_{4i-1}|-\ln|x-\zeta_{4i}|)\right\}. \tag{13}$$

where the dependency of ϕ in Eq. (12) is suppressed by the term $(a/b)^N\to 0$ as $(a/b)<1$ and $N\to\infty$. Eq. (13) indicates that not only image singularities at ζ_{4i-3}, ζ_{4i-2}, ζ_{4i-1} and ζ_{4i}, $i\in N$, but also one singularity of $((\ln b-\ln R_\zeta)/(\ln b-\ln a))\ln\rho$ at the origin and two rigid body terms of $2N\ln(R_\zeta/a)$ and $((\ln R_\zeta-\ln a)/(\ln b-\ln a))\ln b$ for the fixed–fixed case are required. The Green's function in Eq. (13) satisfies the governing equation and boundary conditions at the same time. It is found that a conventional MFS loses a free constant and completeness may be questionable. This also supports that the free constant is important especially in 2-D problem which has been pointed out by Saavedra and Power [33]. Similarly, the image method can be extended to solve fixed–free and free–fixed cases with respect to the inner and outer boundary conditions, respectively. All the series solutions are analytically derived in Table 1 not only for fixed–fixed but also for fixed–free and free–fixed cases.

It is worthy of noting that the mathematical equivalence between coefficients ($c(N)$ and $d(N)$) and interpolation functions can be proved by using the degenerate kernels for three boundary conditions as shown in Table 1. Two ways by using the numerical method and analytical derivation are provided to determine the unknown coefficients. Also, numerical data and analytical formulae are given in Figs. 5–7. It is found that the two equations in Eqs. (10) and (11) are obtained from two different ways. It is proved that they have the same analytical content and numerical results.

The analytical Green's function is shown in Eq. (13) when N approaches infinity. Readers may wonder the term of infinity, $2N\ln(R_\zeta/a)$, as N approaches infinity. A general existence for Eq. (13) can be understood in the following Section 4 which proves the equivalence between the Trefftz solution and Eq. (13). However, we must mention that the sum of infinity term, $\sum_{i=1}^{N}(\ln|x-\zeta_{4i-3}|+\ln|x-\zeta_{4i-2}|-\ln|x-\zeta_{4i-1}|-\ln|x-\zeta_{4i}|)$, and minus infinity $(2N\ln(R_\zeta/a))$ yields a finite value as N approaches infinity in the numerical experiment. A very similar case is shown below: $(\sum_{m=1}^{N}(1/m)-\ln N)=\gamma$, where γ is a finite value of Euler constant.

3. Derivation of the Green's function for an annular case by using the Trefftz method

The problem of annular case in Fig. 8 can be decomposed into two parts. One is infinite plane with a concentrated source (fundamental solution) in Fig. 8(a) and another is annular circles

UNCORRECTED PROOF

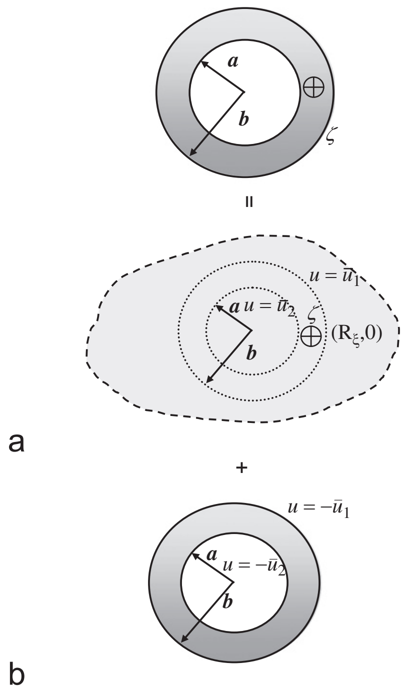

Fig. 8. Sketch of superposition approach. (a) An infinite plan with a concentration source and (b) an annular circles subject to specified boundary conditions.

subject to specified boundary conditions as shown in Fig. 8(b). The first part solution can be obtained from the fundamental solution as follows:

$$G_F(x,\zeta)=\frac{\ln|x-\zeta|}{2\pi} \tag{14}$$

In the image method, all the singularities are put outside the domain to satisfy the specified BC of the second part solution. This is the reason why we call the image method is a special case of MFS. Here, the second part is solved by using the Trefftz method. The solution can be superposed by using the Trefftz base as shown below:

$$G_T(x,\zeta)=\sum_{j=1}^{N_T} c_j \Phi_j \tag{15}$$

where Φ_j is the jth T-complete function and N_T is the number of T-complete function. Here, the T-complete functions are given as 1, $\rho^m \cos m\phi$ and $\rho^m \sin m\phi$ for the interior case and $\ln\rho$, $\rho^{-m}\cos m\phi$ and $\rho^{-m}\sin m\phi$ for the exterior case. The Green's function can be represented by

$$G_T(x,\zeta)=p_0+\bar{p}_0\ln\rho+\sum_{m=1}^{\infty}[(p_m\rho^m+\bar{p}_m\rho^{-m})\cos m\phi + (q_m\rho^m+\bar{q}_m\rho^{-m})\sin m\phi] \tag{16}$$

where $x=(\rho,\phi)$, p_0, $\bar{p}_0$, p_m, $\bar{p}_m$, q_m and $\bar{q}_m$ are unknown coefficients. By matching the boundary conditions, we substitute $x=(a,\phi)$ and $x=(b,\phi)$ in Eq. (15) to determine the unknown coefficients. Then, the series-form Green's function is obtained by superimposing the solutions of $G_F(x,\zeta)$ and $G_T(x,\zeta)$ as shown below

$$G(x,\zeta)=\frac{\ln|x-\zeta|}{2\pi}-(b\ln b p_0+a\ln\rho\,\bar{p}_0)+\sum_{m=1}^{\infty}\frac{1}{2m}\left[\left(\frac{\rho^m}{b^{m-1}}p_m+\frac{a^{m+1}}{\rho^m}\bar{p}_m\right)\cos m\phi+\left(\frac{\rho^m}{b^{m-1}}q_m+\frac{a^{m+1}}{\rho^m}\bar{q}_m\right)\sin m\phi\right], \tag{17}$$

where the unknown coefficients are obtained,

$$\begin{Bmatrix} p_0 \\ \bar{p}_0 \end{Bmatrix}=\begin{Bmatrix} \dfrac{\ln a-\ln R_\zeta}{2\pi b(\ln a-\ln b)} \\ \dfrac{\ln b-\ln R_\zeta}{2\pi a(\ln b-\ln a)} \end{Bmatrix}, \tag{18}$$

$$\begin{Bmatrix} p_m \\ \bar{p}_m \end{Bmatrix}=\begin{Bmatrix} \dfrac{b^{m-1}\cos m\theta[b^m(R_\zeta/b)^m-a^m(a/R_\zeta)^m]}{(b^{2m}-a^{2m})\pi} \\ \dfrac{b^m\cos m\theta[b^m(a/R_\zeta)^m-a^m(R_\zeta/b)^m]}{a(b^{2m}-a^{2m})\pi} \end{Bmatrix},\quad m=1,2,3,\ldots, \tag{19}$$

$$\begin{Bmatrix} q_m \\ \bar{q}_m \end{Bmatrix}=\begin{Bmatrix} \dfrac{b^{m-1}\sin m\theta[b^m(R_\zeta/b)^m-a^m(a/R_\zeta)^m]}{(b^{2m}-a^{2m})\pi} \\ \dfrac{b^m\sin m\theta[b^m(a/R_\zeta)^m-a^m(R_\zeta/b)^m]}{a(b^{2m}-a^{2m})\pi} \end{Bmatrix},\quad m=1,2,3,\ldots. \tag{20}$$

Therefore, the series-form Green's functions are obtained in Table 1 for the three cases. For simplicity and without loss of generality, we prove the equivalence for the fixed–fixed case in the next section.

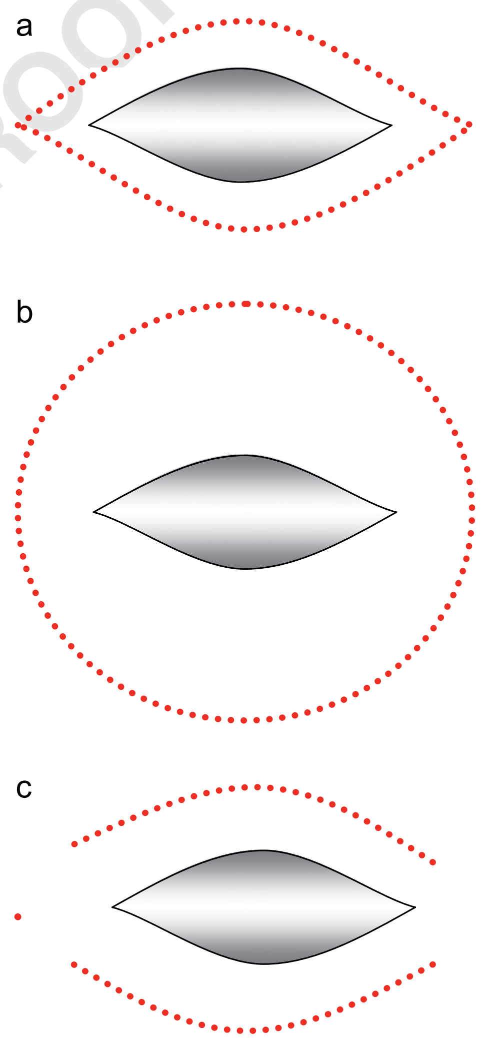

Fig. 9. Optimal locations for the MFS [35]. (a) Expansion, (b) circle and (c) lump (optimal case).

UNCORRECTED PROOF

4. Mathematical equivalence between the MFS and Trefftz method

4.1. Method of fundamental solutions (image method)

The image method can be seen as a special case of MFS, since its singularities are located outside the domain for the second part solution in Fig. 8(b). The Green's function of Eq. (13) can be expanded into series form by separating the field point $x(\rho,\phi)$ and source point $s(R,\theta)$ for the fundamental solution in the polar coordinate of Eq. (8) as shown below

$$G(x,\zeta)=\frac{1}{2\pi}\left[\ln|x-\zeta|-\frac{\ln R_\zeta-\ln a}{\ln b-\ln a}\ln b-\frac{\ln b-\ln R_\zeta}{\ln b-\ln a}\ln\rho\right]-\frac{1}{2\pi}\sum_{i=1}^{\infty}\sum_{m=1}^{\infty}\frac{1}{m}\left[\left(\frac{\rho}{\zeta_{4i-3}}\right)^m+\left(\frac{\zeta_{4i-2}}{\rho}\right)^m-\left(\frac{\zeta_{4i-1}}{\rho}\right)^m-\left(\frac{\rho}{\zeta_{4i}}\right)^m\right]\cos m(\theta-\phi). \tag{21}$$

Without the loss of generality, the source in the annular domain can be chosen as $\zeta=(R_\zeta,0)$. By using Eqs. (4) and (5), the series results in four geometric series with the common ratio of a^2/b^2 which is less than one in Eq. (13) and can be rearranged into

$$G(x,\zeta)=\frac{\ln|x-\zeta|}{2\pi}+\frac{1}{2\pi}\sum_{m=1}^{\infty}\frac{1}{m}\left[\frac{R_\zeta^{2m}\rho^{2m}+a^{2m}b^{2m}-a^{2m}R_\zeta^{2m}-a^{2m}\rho^{2m}}{R_\zeta^m\rho^m(b^{2m}-a^{2m})}\right]\cos m\phi-\frac{1}{2\pi}\frac{\ln R_\zeta-\ln a}{\ln b-\ln a}\ln b-\frac{1}{2\pi}\frac{\ln b-\ln R_\zeta}{\ln b-\ln a}\ln\rho,\quad a\leqslant\rho\leqslant b, \tag{22}$$

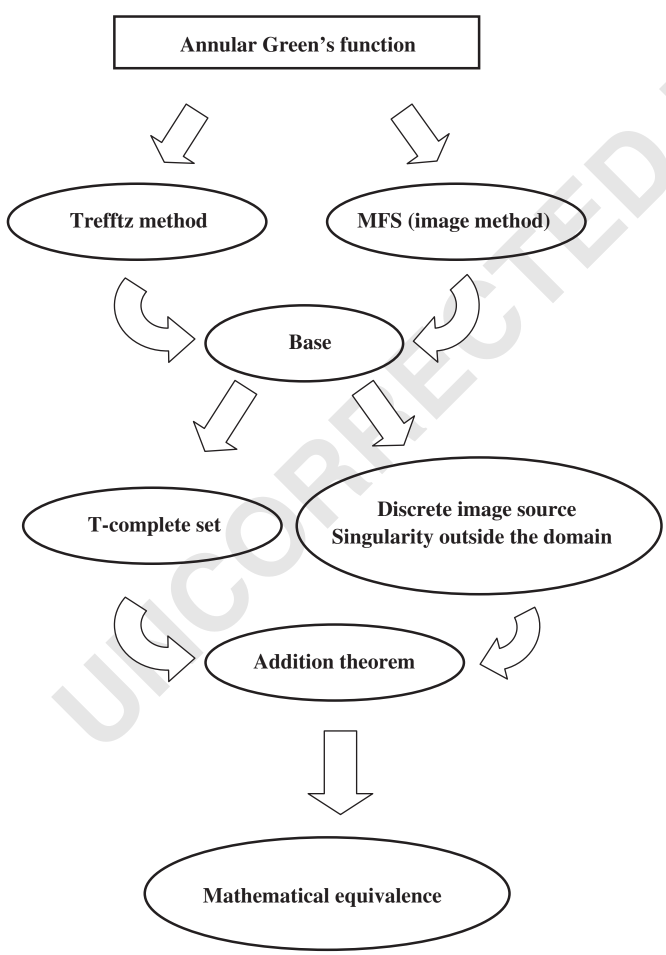

Fig. 10. Equivalence between the Trefftz method and MFS (image method).

after expanding all the image singularities of ln functions. Regarding the optimal location for singularities of MFS for the second part solution in Fig. 8(b), it is interesting to find that the optimal location may not be the expansion type of Fig. 9(a) or angular distribution of Fig. 9(b), but a lump singularity in one radial direction as shown in Fig. 9(c) as mentioned by Alves and Antunes [35]. In this paper, our image location in the MFS only lumps on the radial direction which agrees with the optimal location in [34,35].

4.2. The Trefftz method

Since the angle of source location can be set to zero without loss of generality, the coefficients of Eqs. (19) and (20) can be simplified to

$$\begin{Bmatrix} p_m \\ \bar{p}_m \end{Bmatrix}=\begin{Bmatrix} \dfrac{b^{m-1}[b^m(R_\zeta/b)^m-a^m(a/R_\zeta)^m]}{(b^{2m}-a^{2m})\pi} \\ \dfrac{b^m[b^m(a/R_\zeta)^m-a^m(R_\zeta/b)^m]}{a(b^{2m}-a^{2m})\pi} \end{Bmatrix},\quad m=1,2,3,\ldots, \tag{23}$$

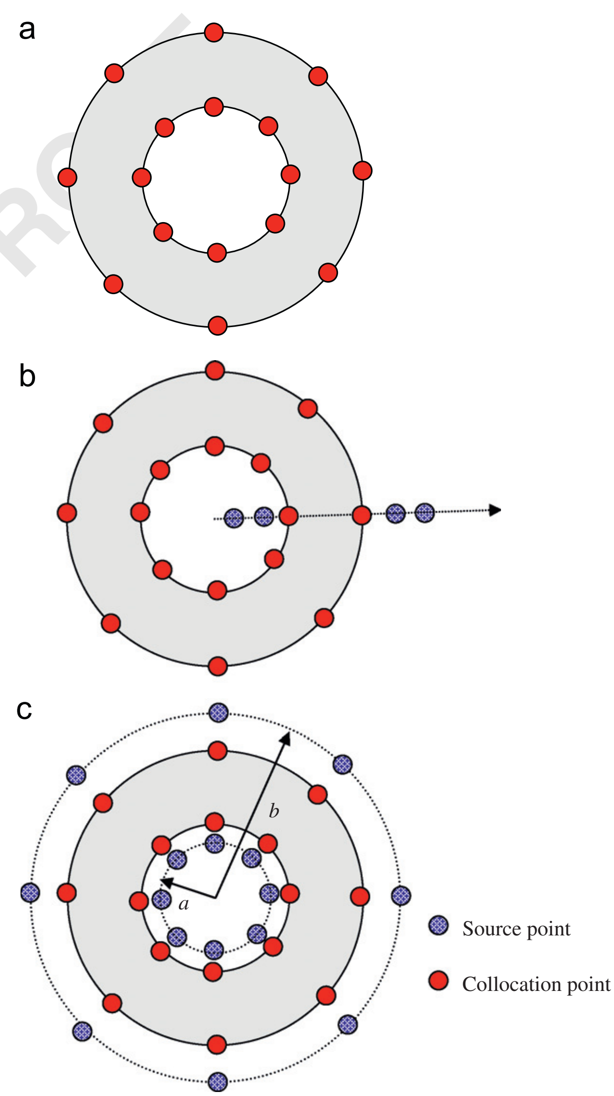

Fig. 11. Sketches of (a) the Trefftz method, (b) the image method (special MFS, radial distribution of singularities) and (c) conventional MFS (angular distribution of singularities).

UNCORRECTED PROOF

$$\begin{Bmatrix} q_m \\ \bar{q}_m \end{Bmatrix} = \begin{Bmatrix} 0 \\ 0 \end{Bmatrix}, \quad m = 1, 2, 3, \ldots. \tag{24}$$

Then, the Green's function in Eq. (17) can be rewritten as

$$G(x,\zeta) = \frac{\ln|x-\zeta|}{2\pi} + \frac{1}{2\pi}\sum_{m=1}^{\infty}\frac{1}{m}\left[\frac{R_\zeta^{2m}\rho^{2m} + a^{2m}b^{2m} - a^{2m}R_\zeta^{2m} - a^{2m}\rho^{2m}}{R_\zeta^{m}\rho^{m}(b^{2m}-a^{2m})}\right]\cos m\phi$$
$$-\frac{1}{2\pi}\frac{\ln R - \ln a}{\ln b - \ln a}\ln b - \frac{1}{2\pi}\frac{\ln b - \ln R}{\ln b - \ln a}\ln\rho, \quad a \leqslant \rho \leqslant b. \tag{25}$$

After comparing Eq. (22) with Eq. (25), it is found that the two solutions, Eqs. (13) and (17) have been proved to be mathematically equivalent by using the addition theorem when the number of images and the number of Trefftz bases are both infinite. The equivalence of solutions using the Trefftz method and MFS (image method) is summarized in a flowchart of Fig. 10. Similarly, the mathematical proof of the equivalence between Trefftz and MFS solutions can be extended to fixed–free and free–fixed cases without any difficulty. All the results are shown in Table 1. It is noted that Eq. (22) is obtained from Eq. (13) by expanding the ln singularity using the addition theorem. Eq. (22) is found to be equivalent to the solution of Trefftz method in Eq. (25). Existence

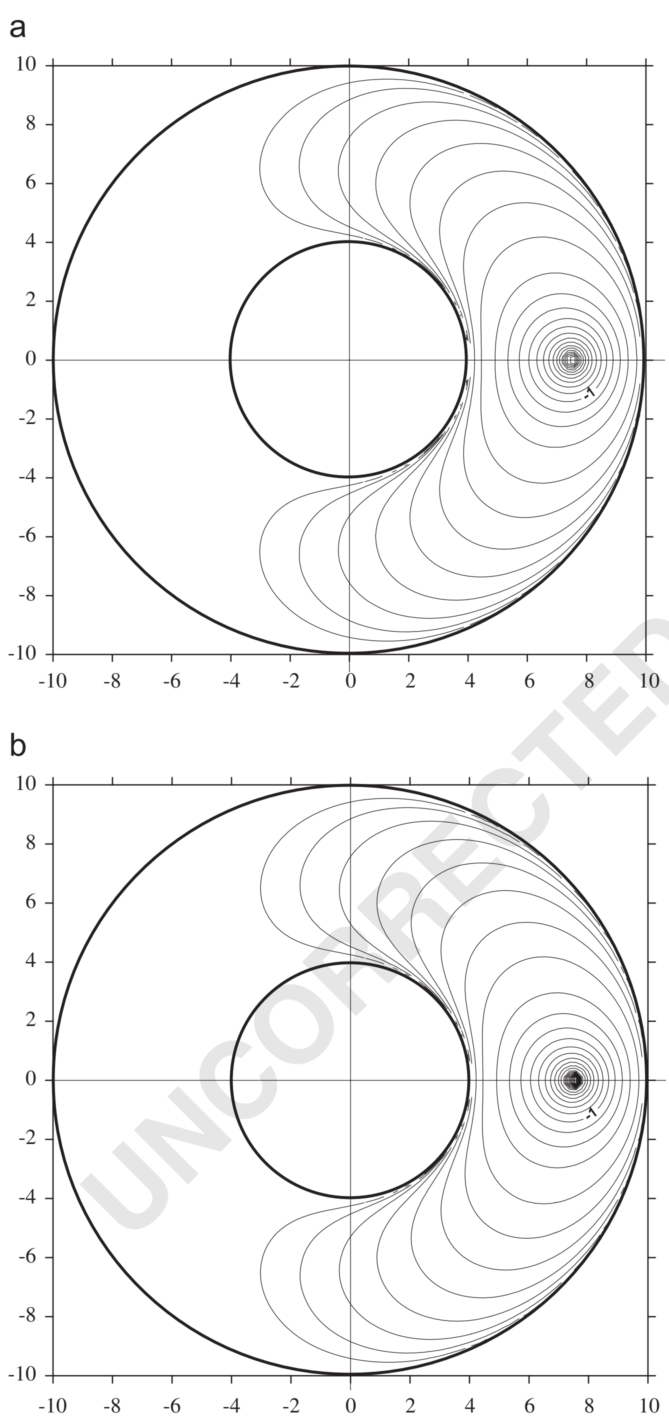

Fig. 12. Contour plot for the analytical solutions (fixed–fixed boundary condition). (a) The Trefftz method and (b) the image method.

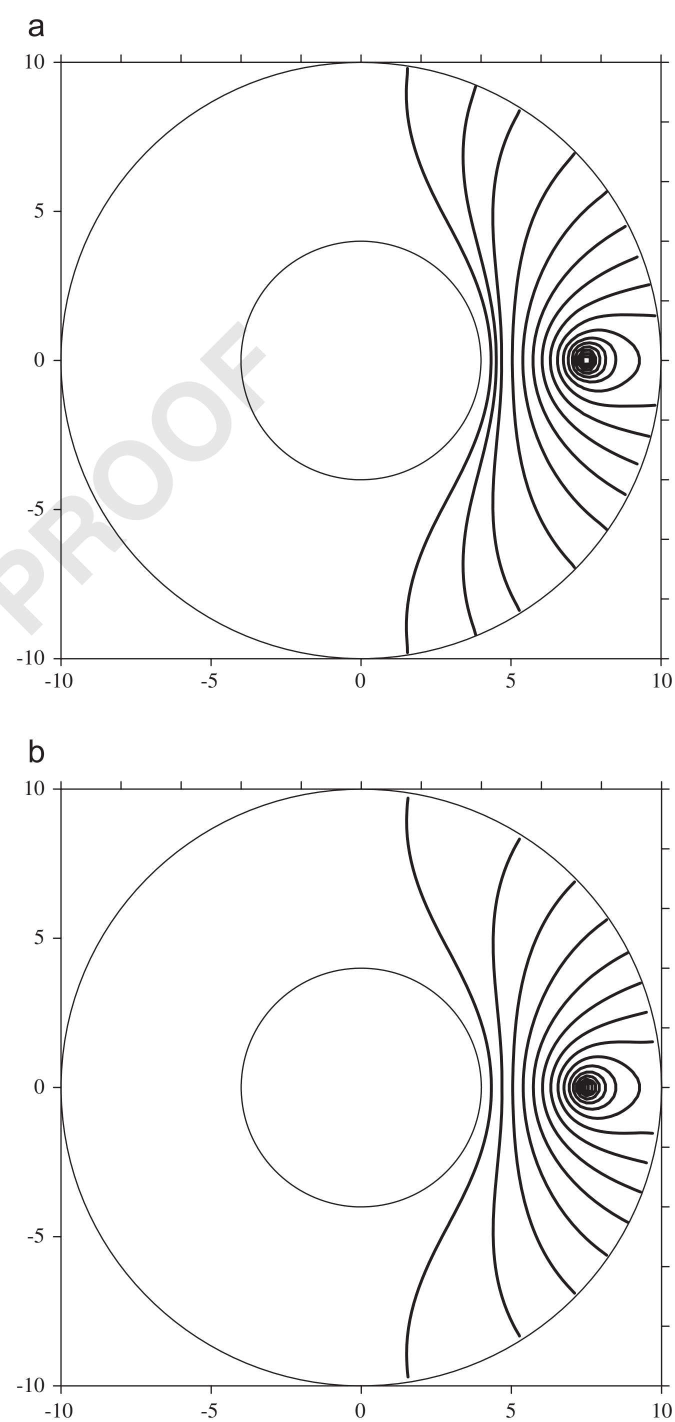

Fig. 13. Contour plot for the analytical solutions (fixed-free boundary condition). (a) The Trefftz method and (b) the image method.

UNCORRECTED PROOF

of Eq. (13) as $N\to\infty$ and series convergence of Trefftz solution of Eq. (25) will be demonstrated in the next section.

5. Illustrative example and discussions

For simplicity, an annular problem subject to the Dirichlet boundary condition is considered here where the source is located at $\zeta = (7.5,0)$. The two radii of inner and outer circles are 4.0 and 10.0, respectively. Although the Trefftz solution and MFS solution (image method) are proved to be mathematically equivalent in the infinite dimension ($N\to\infty$ and $N_T\to\infty$), they are not fully

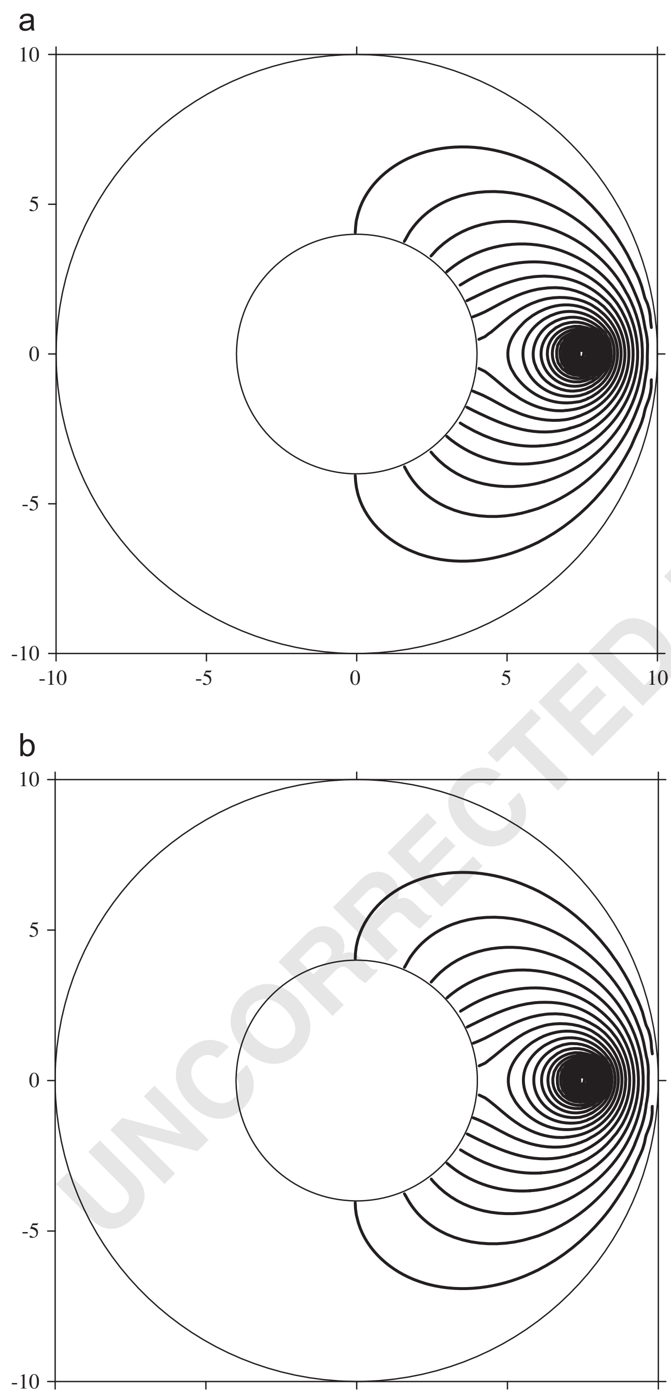

Fig. 14. Contour plot for the analytical solutions (free–fixed boundary condition). (a) The Trefftz method and (b) the image method.

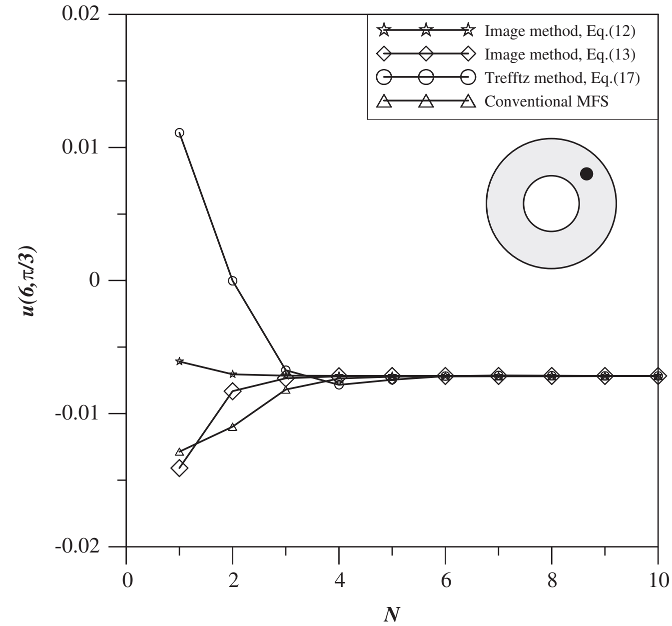

Fig. 15. Pointwise convergence test for the potential $u(6, \frac{\pi}{3})$ by using various approaches.

equivalent in the error analysis. The convergence rate under the same number of degrees of freedoms is an interesting topic. Three approaches, (a) the Trefftz method, (b) special MFS (images method) and (c) MFS with angular singularities (conventional MFS), are considered here. Their distributions of source and collocation points are shown in Fig. 11. The contour plots of analytic solutions using the Trefftz method and image method are shown in Figs. 12–14 for fixed–fixed, fixed–free and free–fixed cases, respectively. Fig. 15 shows the potential at the point $(6,\pi/3)$ versus the number of terms by using various approaches. It is found that the convergence rate of image method is better than those of the Trefftz method and conventional MFS. However, the accuracy of Trefftz method is the worst. Fig. 16 shows the normal derivatives along outer and inner boundaries. The norm error of normal derivatives for outer and inner boundaries versus the number of terms ($N_T = M$) is shown in Fig. 17. Also, the accuracy of the image method is better than those of the conventional MFS and the Trefftz method.

In this example, all the three figures (Figs. 15–17) indicate that the image method is more efficient than MFS with angular singularities and the Trefftz method. The reason can be explained that source points in MFS has been optimally selected by using the image concept. According to the addition theorem, the Trefftz bases are all imbedded in the degenerate kernel. Trefftz bases and ln$r$ singularity with extra constant are both complete for representing the solution. Although it is proved that the solution derived by using the image method and the Trefftz method are mathematically equivalent when the number of degrees of freedom is infinite. Nevertheless, their numerical efficiencies are different on the same number of degree of freedoms. Here, we find that the accuracy of radial distribution of singularity is better than that of the angular distribution in the MFS. Also, we find that the bases of MFS are more efficient than that of the Trefftz method in the fixed–fixed cases.

UNCORRECTED PROOF

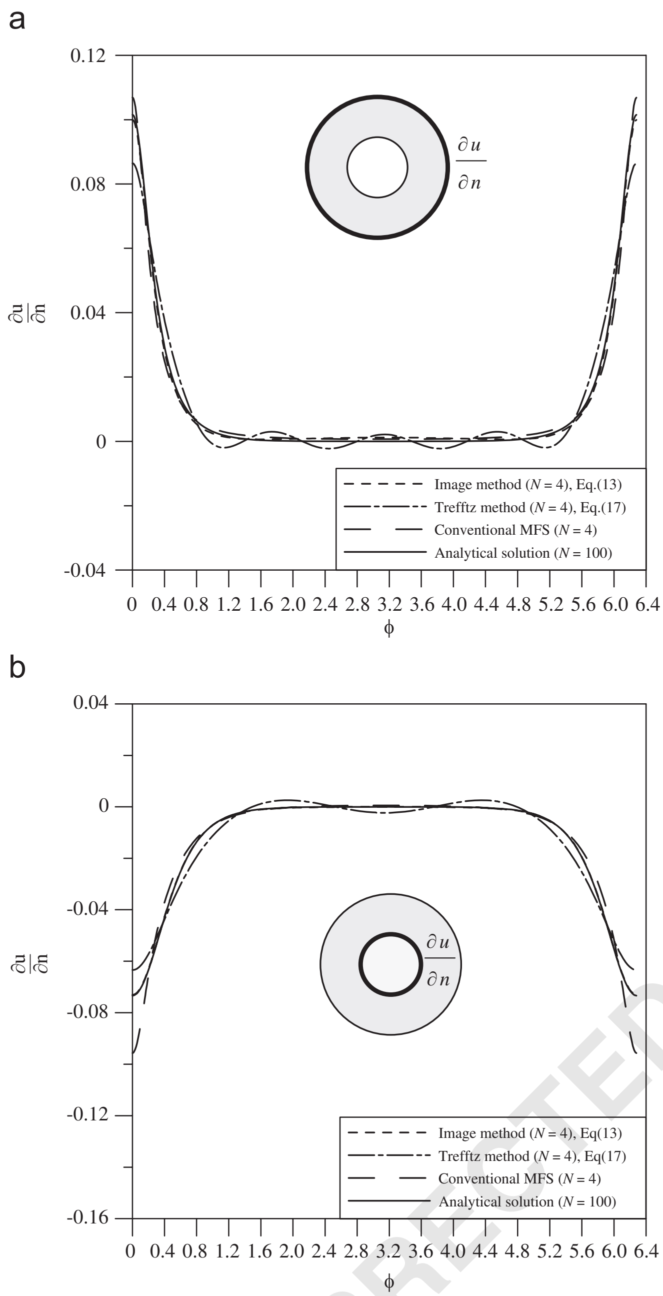

Fig. 16. Normal derivatives along the inner and outer boundaries by using various approaches. (a) Outer boundary and (b) inner boundary.

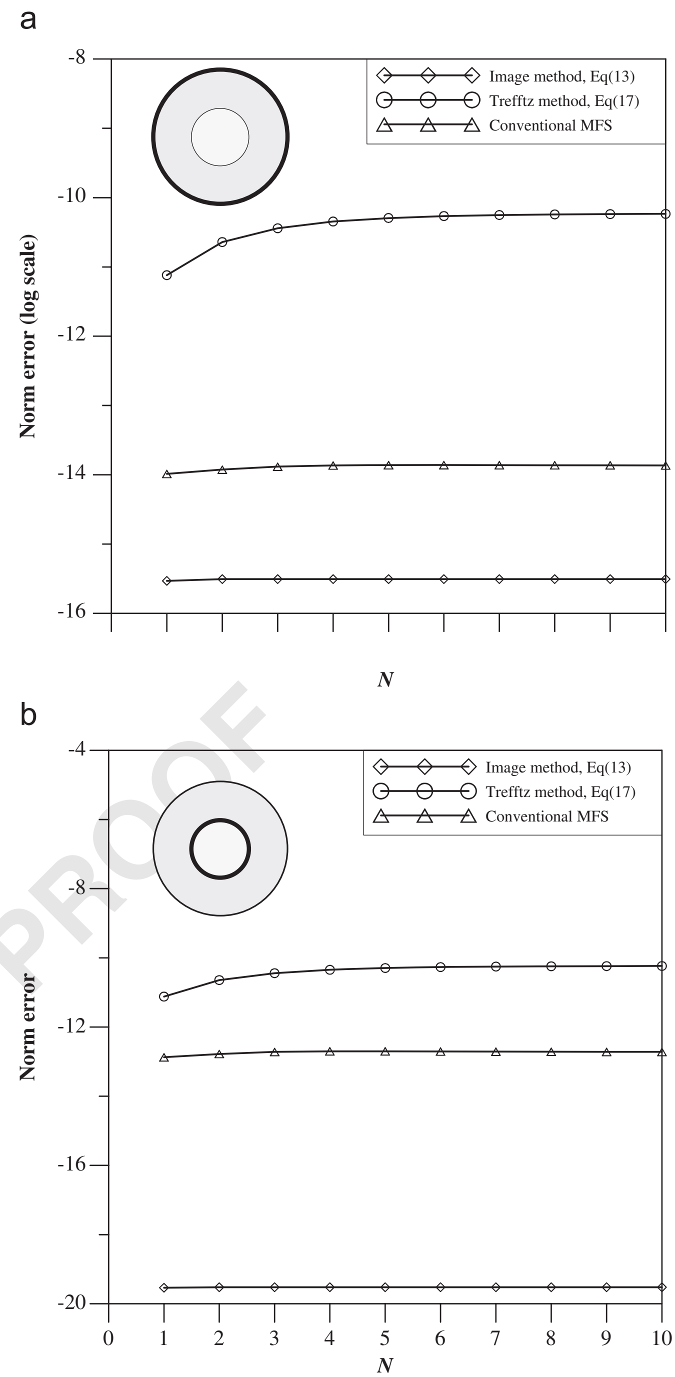

Fig. 17. L^2 norm error $(\int_0^{2\pi}|u(x)-\hat{u}(x)|^2 d\theta)$ versus number of terms. (a) Outer boundary and (b) inner boundary.

UNCORRECTED PROOF

6. Concluding remarks

In this paper, not only the image method (a special MFS) but also the Trefftz method were employed to solve the Green's function of annular Laplace problem. Three cases, fixed–fixed, fixed–free and free–fixed were considered. The two solutions using the Trefftz method and MFS were proved to be mathematically equivalent by using addition theorem or so-called degenerate kernel. On the basis of finite number of degrees of freedoms, the results of image method are found to converge faster than those of the Trefftz method and MFS with angular singularities. Also, the solution of image method shows the existence of the free constant which is always overlooked in the conventional MFS. Finally, we also found the final two frozen image points at the origin and infinity where their strengths can be determined numerically and analytically in a consistent manner.

References

[1] Kita E, Kamiya N. Trefftz method: an overview. Adv Eng Softw 1995;24:3–12.
[2] Jin WG, Cheung YK. Trefftz direct method. Adv Eng Softw 1995;24:65–9.
[3] Chang JR, Liu RF, Yieh WC, Kuo SR. Applications of the direct Trefftz boundary element method to the free-vibration problem of a membrane. J Acoust Soc Am 2002;112(2):518–27.
[4] Jin WG, Cheung YK, Zienkiewicz OC. Application of the Trefftz method in plane elasticity problems. Int J Numer Methods Eng 1990;30:1147–61.
[5] Jin WG, Cheung YK, Zienkiewicz OC. Trefftz method for Kirchhoff plate bending problems. Int J Numer Methods Eng 1993;36:765–81.

[6] Jirousek J, Wroblewski A. T-elements: state of the art and future trends. Arch Comput Methods Eng 1996;3(4):323–434.
[7] Liu CS. An effectively modified direct Trefftz method for 2D potential problems considering the domain's characteristic length. Eng Anal Bound Elem 2007;31:983–93.
[8] Kupradze VD. A method for the approximate solution of limiting problems in mathematical physics. Comput Math Math Phys 1964;4:199–205.
[9] Karageorghis A, Fairweather G. The method of fundamental solutions for axisymmetric potential problems. Int J Numer Methods Eng 1999;44:1653–69.
[10] Fairweather G, Karageorghis A. The method of fundamental solutions for elliptic boundary value problems. Adv Comput Math 1998;9:69–95.
[11] Karageorghis A, Fairweather G. The method of fundamental solutions for the numerical solution of the biharmonic equation. J Comput Phys 1987;69(2):434–59.
[12] Karageorghis A, Fairweather G. The Almansi method of fundamental solutions for solving biharmonic problems. Int J Numer Methods Eng 1988;26:1665–82.
[13] Karageorghis A, Fairweather G. The simple layer potential method of fundamental solutions for certain biharmonic problem. Int J Numer Methods Fluids 1989;9:1221–34.
[14] Jaswon MA, Symm GT. Integral equation methods in potential theory and electrostatics. New York: Academic Press; 1977.
[15] Melnikov YA. Some application of the Green's function method in mechanics. Int J Solids Struct 1977;13:1045–58.
[16] Telles JCF, Castor GS, Guimaraes S. Numerical Green's function approach for boundary elements applied to fracture mechanics. Int J Numer Methods Eng 1995;38(19):3259–74.
[17] Guimaraes S, Telles JCF. General application of numerical Green's functions for SIF Computations with boundary elements. Comput Meth Eng Sci 2000;1(3):131–9.
[18] Ang WT, Telles JCF. A numerical Green's function for multiple cracks in anisotropic bodies. J Eng Math 2004;49:197–207.
[19] Melnikov YA. A basis for computation of thermo-mechanical fields in elements of constructions of complex con figuration. Thesis Dr. Technical Sciences, Moscow Institute of Civil Engineering; 1982. (in Russian).
[20] Melnikov YA. Green's functions in applied mechanics. Boston-Southampton: Computational Mechanics Publications; 1995.
[21] Melnikov YA, Melnikov MY. Modified potential as a tool for computing Green's functions in continuum mechanics. CMES 2001;2:291–305.
[22] Melnikov YA, Melnikov MY. Green's functions for mixed boundary value problems in regions of irregular shape. Electron J Bound Elem 2006;4:82–104.
[23] Thomson W. Maxwell in his treatise. Vol. I., Chapter XI, quotes a paper in the Cambridge and Dublin Math. Journal of 1848, 1848.
[24] Chen JT, Wu CS. Alternative derivations for the Poisson integral formula. Int J Math Educ Sci Technol 2006;37:165–85.
[25] Boley BA. A method for the construction of Green's functions. Q Appl Math 1956;14:249–57.
[26] Adewale AO. Isotropic clamped-free thin annular plate subjected to a concentrated load. J Appl Mech 2006;73(4):658–63.
[27] Chen JT, Ke JN. Derivation of anti-plane dynamic Green's function for several circular inclusions with imperfect interfaces. Comput Model Eng Sci 2008;29(3):111–35.
[28] Courant R, Hilbert D. Methods of mathematical physics. New York: Interscience; 1953.
[29] Schaback R. Adaptive numerical solution of MFS systems. A plenary talk at the first Inter Workshop on the Method of Fundamental Solution, Ayia Napa, Cyprus, June 11–13; 2007.
[30] Bogomolny A. Fundamental solutions method for elliptic boundary value problems. SIAM J Numer Anal 1985;22(4):644–69.
[31] Li ZC, Lu TT, Hu HY, Cheng AHD. Trefftz and collocation methods. Boston-Southampton: WIT Press; 2007.
[32] Chen JT, Wu CS, Lee YT, Chen KH. On the equivalence of the Trefftz method and method of fundamental solutions for Laplace and biharmonic equations. Comput Math Appl 2007;53:851–79.
[33] Saavedra I, Power H. Multipole fast algorithm for the least-squares approach of the method of fundamental solutions for three-dimensional harmonic problems. Numer Methods Partial Differ Equ 2003;19(6):825–45.
[34] Alves CJS, Antunes PRS. The method of fundamental solutions applied to the calculation of eigenfrequencies and eigenmodes of 2D simply connected shapes. CMC 2005;2(4):251–65.
[35] Alves CJS, Antunes PRS. The method of fundamental solutions applied to the calculation of eigensolutions for 2D plates. Int J Num Meth Eng 2008 [accepted].

UNCORRECTED PROOF